Magnetic Assembly of Magnetite/Perovskite Hybrid Nanorods for Circularly Polarized Luminescence

Yucong Su¹, Yuchen Zhang², Zuyang Ye¹, Jolene Cao¹, Qingsong Fan¹, Xinchao Wang³, Chen Chen¹, Yun Liu¹, Zhongxiang Wang¹, Zhenda Lu², and Yadong Yin*¹

Y. Su, Z. Ye, J. Cao, Dr. Q. Fan, C. Chen, Dr. Y. Liu, Z. Wang, Prof. Y. Yin

Department of Chemistry, University of California, Riverside, California 92521, United States

E-mail: yadong.yin@ucr.edu

Y. Zhang, Prof. Z. Lu

College of Engineering and Applied Sciences, Jiangsu Key Laboratory of Artificial Functional Materials Institution, Nanjing University, Nanjing, 210023 P. R. China

X. Wang

Department of Mechanical Engineering, University of Wisconsin-Madison, Madison, WI 53706, United States

KEYWORDS: magnetic assembly, chirality, perovskite, nanostructures, circularly polarized luminescence

Abstract

Magnetic fields are uniquely valuable for creating colloidal nanostructured materials, not only providing a means for controlled synthesis but also guiding their self-assembly into distinct superstructures. In this study, we report a magnetothermal process for synthesizing hybrid nanostructures comprising ferrimagnetic magnetite nanorods coated with fluorescent perovskite nanocrystals and demonstrate their magnetic assembly into superstructures capable of emitting linear and circularly polarized light. Under UV excitation, the superstructures assembled in a liner magnetic field produce linear polarized luminescence, and those assembled in a chiral magnetic field exhibit strong circularly polarized luminescence (CPL) with a g_{lum} value up to 0.44 (±0.004). The CPL is believed to originate from the dipolar interaction between neighboring perovskite nanocrystals attached to the chiral assemblies and the chiral-selective absorption of the perovskite emission by the magnetite phase. The magnetic synthesis and assembly approaches and the resulting distinctive chiral superstructures are anticipated to open up new avenues for designing diverse functional chiroptical devices.

1 Introduction

Chirality, a fundamental property of living organisms in nature, refers to the phenomenon that an object cannot be identical to its mirror image. With non-centrosymmetric structures, chiral materials exhibit various intriguing physical properties such as circular dichroism (CD), circularly polarized photoluminescence (CPL), nonlinear optical (NLO) effects, ferroelectricity, and spin-related properties^[1] making them valuable in many chiroptoelectronic applications, including photodetectors,^[2-3] polarized light-emitting devices,^[4-5] bioresponsive imaging,^[6] and 3D displays.^[7]

In recent years, halide perovskites have gained traction as a class of highly efficient optical materials for various applications such as light-emitting diodes (LEDs),^[8-9] photonic lasers,^[10-11] photodetectors,^[12-13] and solar cells.^[14-15] Adding chirality to perovskite materials presents many new opportunities to create advanced materials with exceptional optical properties, including especially highly efficient CPL. However, perovskite materials' centrosymmetric chemical structure makes it impossible for chirality to arise intrinsically. As a result, three methods have been proposed to impart chirality to perovskites: (i) surface modification of perovskite nanocrystals (NCs) with chiral ligands,^[16] (ii) utilizing the chiral space group of NCs,^[17] and (iii) assembling perovskite NCs into a chiral configuration.^[18-19]

Despite significant efforts, the chemical and structural modifications carried out using methods (i) and (ii) have only resulted in limited CPL improvement with the luminescence dissymmetry factor of g_{lum} on the order of 10^{-3} to 10^{-2} , which greatly limits the practical applications of these materials. Here g_{lum} is used to quantify the differential emission of left-handed circularly polarized light (L-CPL) and right-handed circularly polarized light (R-CPL), and it is defined as $g_{lum} = 2[I_{L-1}]$

 I_R] / [I_L+I_R], where I_L and I_R are the intensities of L-CPL and R-CPL, respectively. [20] The assembly methods (iii) are promising to induce chirality in perovskite materials, typically achieved through co-assembly of achiral perovskites with a chiral gelator, direct encapsulation of the materials within liquid crystals, or using inorganic silica nanohelices as the chiral templates. However, they may have several drawbacks, such as reduced photoluminescence quantum yield (PLQY) and relatively complex procedures for making chiral templates.

In this article, we report a unique magnetothermal process that can efficiently attach perovskite CsPbBr₃ NCs to the surface of magnetite (Fe₃O₄) nanorods, resulting in the creation of Fe₃O₄@SiO₂/CsPbBr₃ hybrid nanorods. Further, we introduce a magnetic approach that allows them to be rapidly assembled into superstructures that can emit linearly or circularly polarized light, which is fully controllable based on the applied fields. In particular, exposing the colloidal dispersion of the hybrid nanorods to the gradient magnetic field of a cube-shaped permanent magnet creates chiral superstructures. Consistent with our recent discovery of quadrupole field chirality of permanent magnets,^[21-25] the assembly of hybrid nanorods in a gradient magnetic field produces superstructures that inherit the original field chirality. Most importantly, the resulting superstructures exhibit strong CPL signals, with their handedness depending on their position relative to the magnet during assembly.

2 Results and Discussion

Figure 1 schematically illustrates the synthesis process of Fe₃O₄@SiO₂/CsPbBr₃ hybrid nanorods. It starts with the preparation of β-FeOOH nanorods (310 nm × 90 nm, Figure 2a, Figure S1) through the hydrolysis of FeCl₃, followed by their overcoating with a silica shell of a controllable thickness (typically 40 nm, Figure S1) and then reduction to ferrimagnetic Fe₃O₄ (Figure 2b). The silica shell plays a crucial role in maintaining the rod shape during the phase

transition from β-FeOOH to Fe₃O₄ and alleviates the considerable volume shrinkage.^[26] After their surfaces are functionalized with polyvinylpyrrolidone (PVP), the magnetic Fe₃O₄@SiO₂ nanorods are placed under a high-frequency alternating current (AC) magnetic field. The Fe₃O₄ nanorods convert radio frequency energy into heat through hysteresis loss, increasing the surrounding temperature, triggering the formation reaction of perovskite NCs, and anchoring them to the silica surface through chelation with PVP (Figure 2c, Figure S2). Figure S3 shows the FT-IR spectra of PVP and final material Fe₃O₄@SiO₂/CsPbBr₃ nanorods. The FT-IR spectra of PVP demonstrated a stretching vibration of C=O at 1655 cm⁻¹, a clear CN stretching vibration peak at 1290 cm⁻¹, and a CH bending vibrational peak at 1423 cm⁻¹. All these relevant characteristic peaks can be observed in the spectra of Fe₃O₄@SiO₂/CsPbBr₃ nanorods, indicating the chelation between CsPbBr₃ and PVP. TEM (Figure 2c) and XRD (Figure S4) also indicated the existence of CsPbBr₃ NCs on the surface of Fe₃O₄@SiO₂ nanorods. The Fe₃O₄@SiO₂ nanorods show effective magnetothermal heating due to the relatively large hysteresis area displayed in the magnetization (M/H) profile in Figure 2d. The amount of heat dissipated during the sample magnetization reversal is directly proportional to the hysteresis area. Therefore, a larger hysteresis area corresponds to higher energy absorption per unit mass, leading to higher heat production. The resulting Fe₃O₄@SiO₂/CsPbBr₃ hybrid nanorods exhibit strong green photoluminescence (PL), as shown in Figure 2e, indicating that the presence of Fe₃O₄ does not significantly affect the optical properties of perovskites (Figure S5).

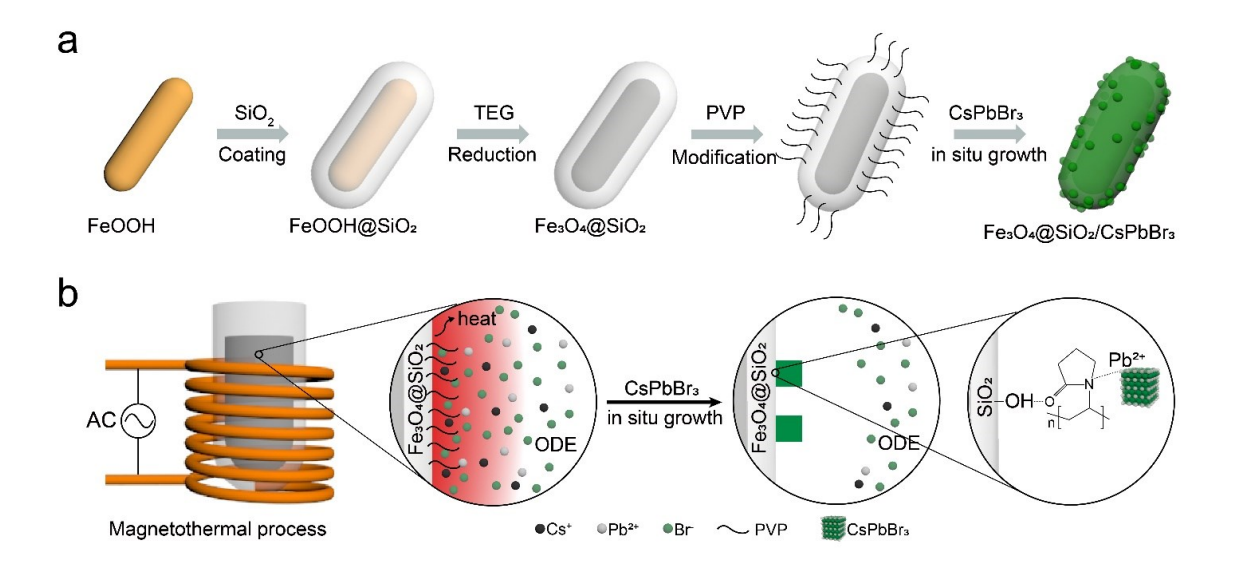


Figure 1. (a, b) Schematic illustration of the magnetothermal synthesis of Fe₃O₄@SiO₂/CsPbBr₃ hybrid nanorods.

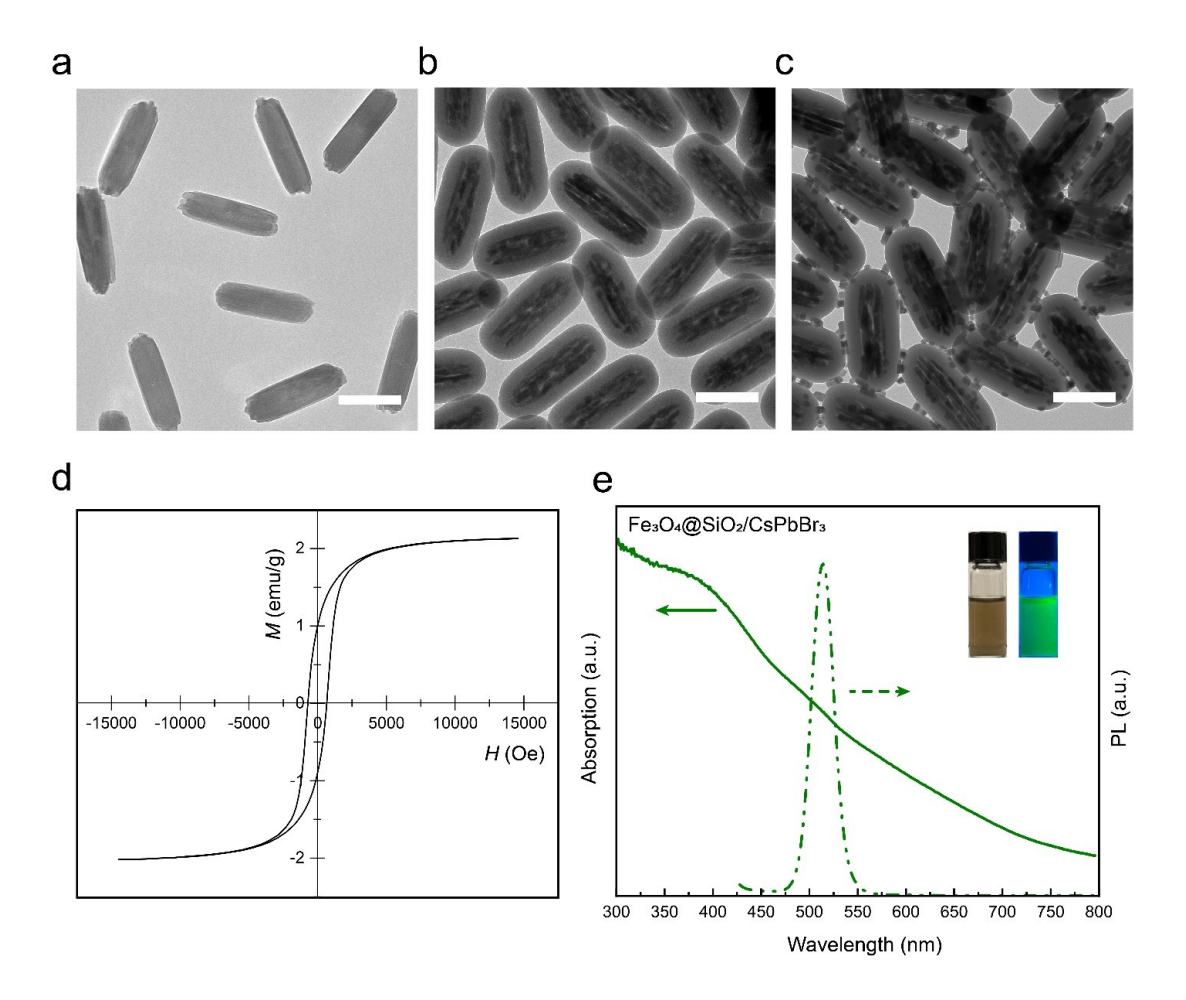


Figure 2. (a) TEM images of β-FeOOH nanorods, (b) Fe₃O₄@SiO₂ nanorods, (c) Fe₃O₄@SiO₂/CsPbBr₃ hybrid nanorods. The scale bars are 200 nm. (d) Magnetic hysteresis curve of Fe₃O₄@SiO₂ nanorods. (e) Absorption and PL spectra of Fe₃O₄@SiO₂/CsPbBr₃ hybrid nanorods. The insets show photographs of hybrid nanorods under natural light and UV light.

The successful synthesis of high-quality Fe₃O₄@SiO₂/CsPbBr₃ hybrid nanorods hinges on two key processes: local magnetothermal heating and PVP functionalization. A high heating rate and elevated reaction temperature (150 °C) are required for the conventional hot-injection synthesis of perovskite NCs. [27] In the current synthesis, these conditions are attained by subjecting Fe₃O₄@SiO₂ nanorods to an alternating magnetic field generated by passing an alternating current of 400 kHz through a solenoid coil. The rapid conversion of electromagnetic energy into thermal energy occurs through Brownian relaxation, Néel relaxation, and hysteresis losses of the magnetic component, with the heating efficiency affected by the size and shape of the magnetic nanoparticles, the strength and frequency of the applied magnetic field, and the collective behavior arising from high particle concentration. [28-29] The magnetothermal heating of Fe₃O₄ nanorods can effectively induce the formation reaction of perovskite by raising the particle surface temperature, instead of the bulk solution, above the reaction threshold, thereby enabling in situ deposition of perovskite NCs onto the nanorod surfaces. As shown in Figure 3a, no CsPbBr₃ formation occurred when the solution was heated to 120 °C using the conventional heating method based on conduction and convection, as it is lower than the required threshold of 150 °C. In contrast, magnetothermal heating produced CsPbBr₃ even when the bulk solution was measured at 120 °C, indicating that the local temperature surrounding the nanorods was above 150 °C. Figure 3b shows the temperature profile of a Fe₃O₄@SiO₂ nanorod in 1-Octadecene (ODE) after magnetothermal

heating for 75 s, as simulated using the finite element method within the COMSOL Multiphysics software package. When the temperature of bulk ODE reaches 120°C, the surface temperature of the nanorod already rises to 155°C, sufficient for triggering perovskite formation. As perovskite formation is limited to near nanorod surface, the local heating benefits preferential surface deposition of CsPbBr₃ NCs to yield high-quality hybrid nanorods.

The PVP modification also plays a crucial role in anchoring perovskite NCs on the nanorod surface. The TEM images in Figure 3d-3g show that an increasing amount of PVP (ranging from 0 wt% to 4 wt%) results in a higher number of perovskite NCs adhering to Fe₃O₄@SiO₂ nanorods. The immobilization of perovskites on the silica surface is facilitated by the chelation between the N atoms in PVP and Pb²⁺ ions in perovskite, thanks to the sp² hybridization of the Pb²⁺ ions and the p π conjugated system with sp² hybridization formed between the N atom and carbonyl group in PVP. [30] Increasing the concentration of PVP in the reaction results in higher PL intensity of the hybrid nanorods, as seen in Figure 3c. This is due to the increase in available chelating sites on the nanorod surface. With continuous increase of PVP concentrations beyond 4 wt%, there was no obvious difference in PL intensity (Figure S6). Further increasing the PVP concentration did not lead to an increase in the amount of attached CsPbBr₃ nanocrystals. With the same amount of PVP used for modification, we synthesized the hybrid nanorods by in-situ growth method and postprocessing method. The simple mixing of preformed perovskite NCs and Fe₃O₄@SiO₂ nanorods resulted in fewer perovskite NCs attached to the nanorod surface compared to in-situ growth using the magnetothermal method, as shown in Figures 3g and 3h. This finding indicates that local heating is beneficial for producing hybrid nanorods with high PL intensity.

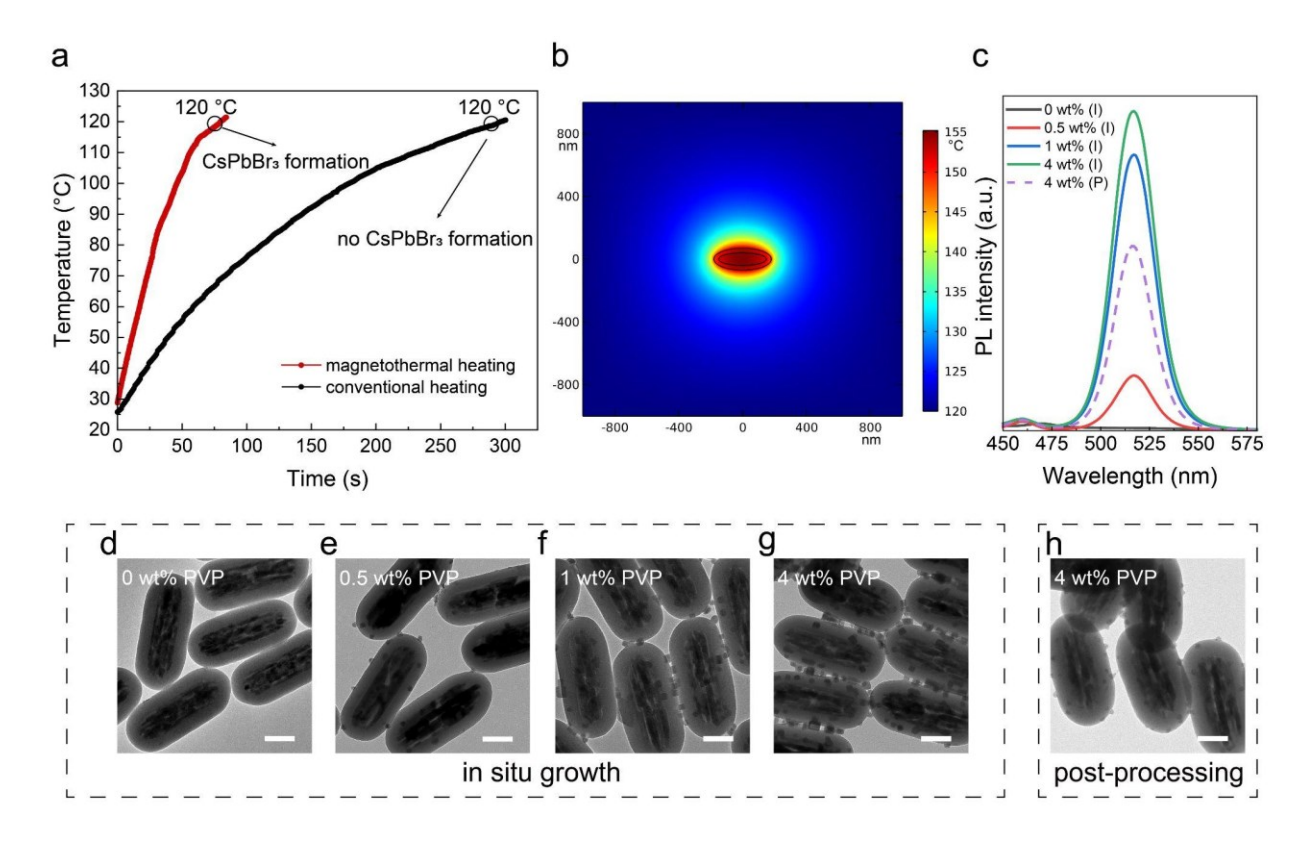


Figure 3. (a) Temperature increase over time by magnetothermal and traditional heating of a colloidal dispersion of Fe₃O₄@SiO₂ nanorods in ODE. (b) Simulated temperature profile of a Fe₃O₄@SiO₂ nanorod in ODE during magnetothermal heating. (c) PL intensity of Fe₃O₄@SiO₂/CsPbBr₃ hybrid nanorods prepared through magnetothermal in situ growth (denoted as I) or post-processing (denoted as P) methods, with the initial Fe₃O₄@SiO₂ nanorods modified by PVP of different concentrations. (d-h) TEM images of the hybrid nanorods corresponding to samples in (c). The scale bars are 100 nm.

We assembled the hybrid nanorods into linearly polarized structures under a parallel magnetic field created using two magnets with opposing poles, as illustrated in **Figure 4a**. The specific process involved mixing hybrid nanorods with a polyurethane-based Norland optical adhesive to produce a well-dispersed liquid mixture. This mixture was then dropped onto a glass substrate and

placed in a parallel magnetic field. UV curing of the optical adhesive then fixed the orientation of the hybrid nanorods. The resulting film was tested using a homemade microscope system illustrated in Figure 4b, exhibiting polarized PL emission as shown in Figure 4c. The polarization test at the emission point (520 nm) can be carried out by adding a removable polarizer. When the polarizer was rotated to different angles from 0° to 360°, the sample's PL spectra were obtained by pro-CCD installed on a spectrometer. The PL intensity at different angles is well fitted with a trigonometric function. The peaks of the fitted curve represent the intensity of the light along the parallel magnetic field direction, while the valleys represent the intensity of the light perpendicular to the field direction. Here, the polarization ratio is defined as the difference between the intensities emitted from the two orthogonal directions. The polarization ratio of the film, defined as (I_{max}- I_{min} // ($I_{max}+I_{min}$), is approximately 0.10 (± 0.002). In one-dimensional (1D) nanomaterials, the dielectric confinement of the optical electric field causes the transition dipole to align along the long axis of the nanorods. As a result, the resulting asymmetric excitons contribute to the optical anisotropy observed in these materials. The generation of linearly polarized light emissions is therefore attributed to the coulomb and dipolar interactions between the adjacent perovskite NCs in the aligned Fe₃O₄@SiO₂ nanorods.

We have recently revealed the chiral distribution of the magnetic field of a cube-shaped permanent magnet and demonstrated that the azimuth of the local magnetic field undergoes gradual changes in each quadrant. [21] **Figure 5b** illustrates the local-field rotation, as represented by the blue arrows, after calculating the differential magnetic field by subtracting the magnetic field vectors in the chosen xy cross sections. The rotation angle is defined as the differences between the azimuth of the magnetic fields in the two cross sections. The differential field exhibits two distinct regions near the N pole: a red region indicating right-handed rotation and a blue region

indicating left-handed rotation. The chirality of the magnetic field is not uniform in these regions, with increasing rotation angle near the N pole.

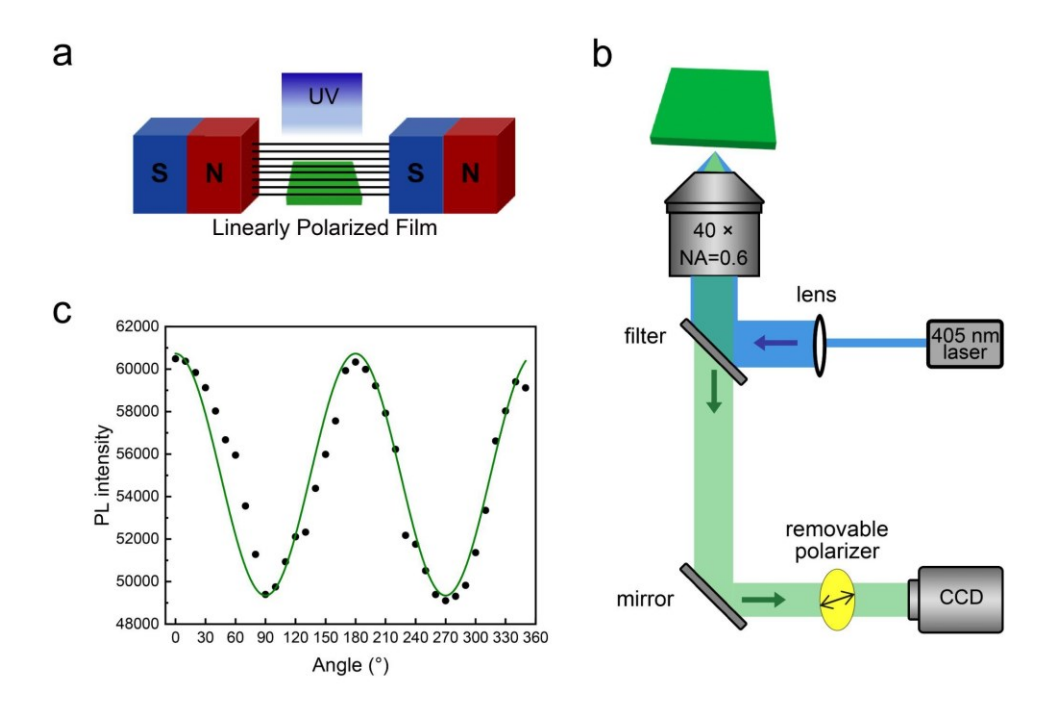


Figure 4. (a) Scheme illustrating the fabrication of linearly polarized film. (b) Scheme illustrating the microscope system for characterizing linear polarization. (c) The polarized PL emission of the linearly polarized film.

Circularly polarized films were fabricated by placing the glass substrates containing hybrid nanorods/optical adhesive mixtures in the right-handed or left-handed quadrants of a permanent magnet, followed by UV curing to fix the nanorod orientations (Figure 5a). As a result, the chirality of the magnetic field was translated into the hybrid nanorod assemblies (Figure 5b), whose chiroptical properties were subsequently characterized using CD spectroscopy. The films prepared in the left-handed and right-handed fields exhibited strong CD signals with opposite directions, as shown in Figure 5c. Linear dichroism (LD) measurement for circularly polarized

film shows a weak LD peak (**Figure S7**), indicating that the observed optical activity primarily arises from the chiral arrangement of the nanorods, with minimal contribution from LD. The scattering effect has been studied in our previous work, where the CD responses were measured in an aqueous solution of glycerol (n = 1.475) with an increasing volume ratio from 0% to 100%. This refractive index-matching experiment demonstrates that both the scattering and absorption of the nanorods contribute to the overall CD responses. Then, we fabricated three L-handed CPL films with different thicknesses (0.3mm, 0.6mm, and 1.0mm) and tested glum at the same relative location. As summarized in **Table S1**, the glum values are almost the same. We therefore tend to conclude that scattering is not a major factor contributing to the overall CD signals. This result confirms the chiral nature of the magnetically assembled hybrid nanorods, given that CD arises from the differential absorption of left-hand and right-hand circularly polarized light.

When excited by light at 405 nm, the films emitted photoluminescence at a wavelength of 520 nm. The emitted light was found to be chiral, and its handedness depended on the location relative to the magnet. **Figure 6a** shows the CPL signal from a film prepared in a left-handed quadrant of a cubic magnet. The measurement was conducted on an optical setup resembling **Figure 4b**, but with a circular polarizer instead of the linear one shown in **Figure S8**. The film was divided into 12 regions, and the CPL was tested in each region. In regions 1 and 5, the intensity of L-CPL was found to be significantly greater than R-CPL, indicating an overall left-handed chirality. Furthermore, the difference between the L-CPL and R-CPL signals decreased as we moved from regions 1 to 4 or from regions 5 to 8. No significant difference was observed in regions 9 to 12. These results are consistent with the magnetic field distribution simulated for the cubeshaped permanent magnet (**Figure 5b**). The chirality was further evaluated using the luminescence dissymmetry factor (g_{lum}), which is defined as $g_{lum} = 2[I_L - I_R] / [I_L + I_R]$ and quantifies the fraction

of circularly polarized light emitted for each handedness. As summarized in **Figure 6b**, the maximum value of g_{lum} reached 0.44 (± 0.004) in region 5, indicating strong CPL in this region. Additionally, g_{lum} decreased from regions 1 to 4 and from regions 5 to 8, suggesting a gradual reduction in CPL intensity. Regions 9 to 12 showed very small g_{lum} , indicating negligible CPL. The results for the film prepared in the right-handed quadrant exhibited a similar location dependence, as presented in **Figure S9**. Overall, the CPL properties measured for both left- and right-handed films are consistent with the chiral field distribution simulated for a cube-shaped permanent magnet.

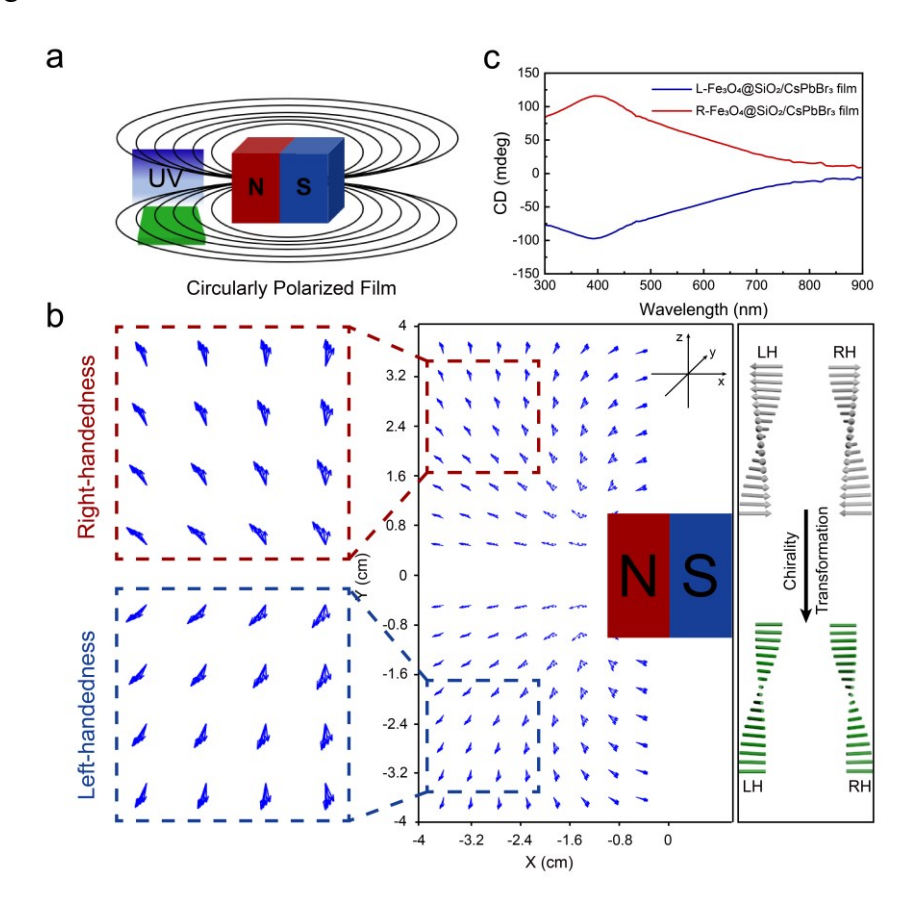


Figure 5. (a) Scheme illustrating the fabrication of circularly polarized film. (b) Distribution of magnetic field with a cubic shape and edge length of 2 cm. The blue arrows are field-rotating vectors. The right panel shows the chirality translation from magnetic field to hybrid nanorod superstructures. (c) CD spectra of left-handed and right-handed circularly polarized films.

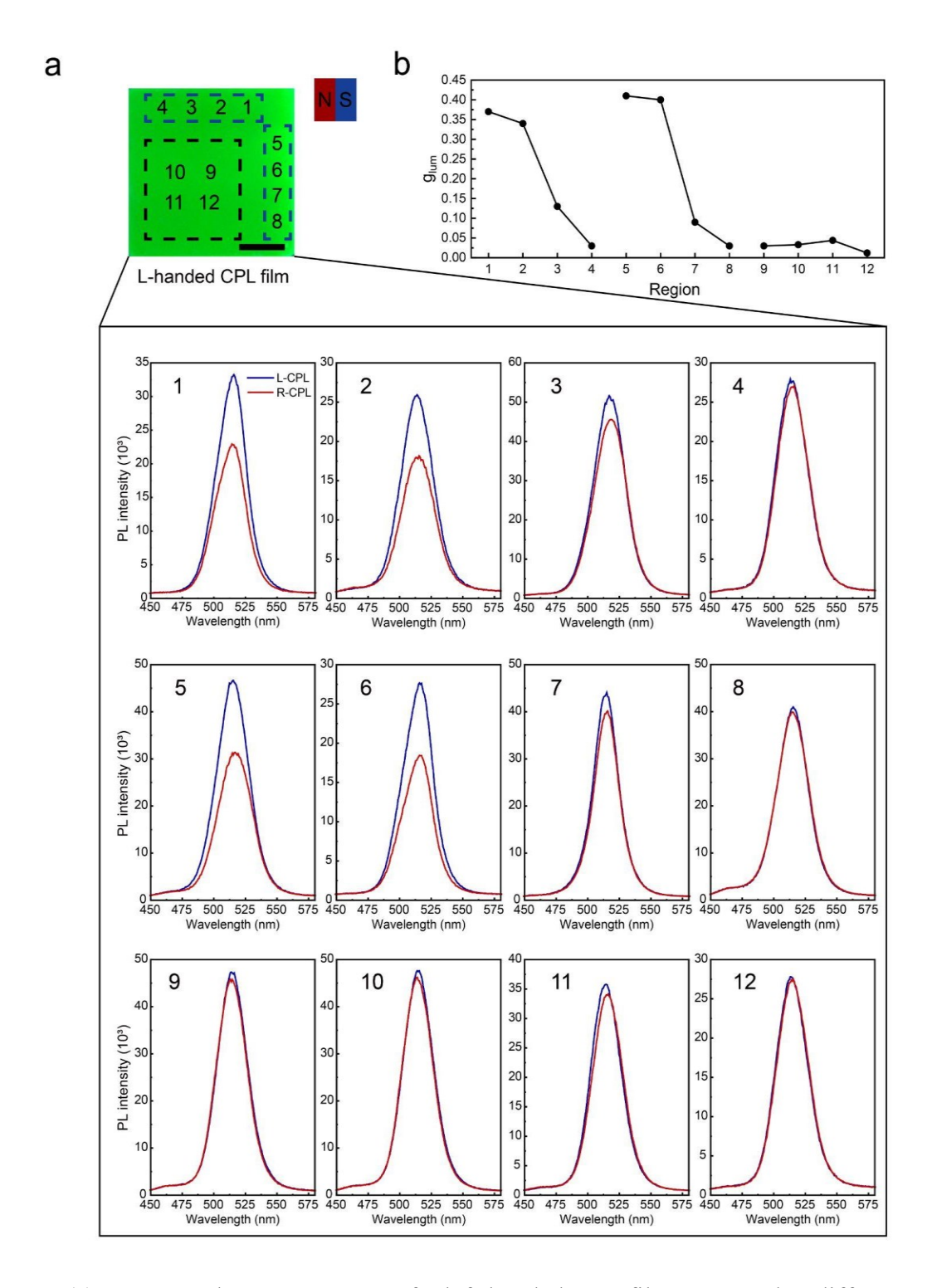


Figure 6. (a) L-CPL and R-CPL spectra of a left-handed CPL film measured at different regions relative to the cubic magnet. The scale bar is 0.5 cm. (b) g_{lum} of left-handed CPL film in different regions.

We suggest two possible explanations for how the chiral assembly of hybrid nanorods can produce CPL in CsPbBr₃. The first one is based on the work of Liu et al. on coupled dipole method (CDM) simulations, ^[19] indicating that CPL arises from the dipolar interaction between CsPbBr₃ nanocrystals that are arranged in a chiral configuration (Figure 7a). According to this mechanism, the amplitude of the CPL signal strongly depends on the grafting density of the NCs and their interparticle distances. This is evidenced in Figure S10, where superstructures grafted with a high density of CsPbBr₃ NCs exhibited considerable differences in left-handed and right-handed CPL intensity. In contrast, those with a low density did not exhibit a preference for CPL signals. At sufficiently low grafting density, CPL signals were not observable as the electromagnetic interaction between CsPbBr₃ NCs diminished quickly with the increase of interparticle distances.

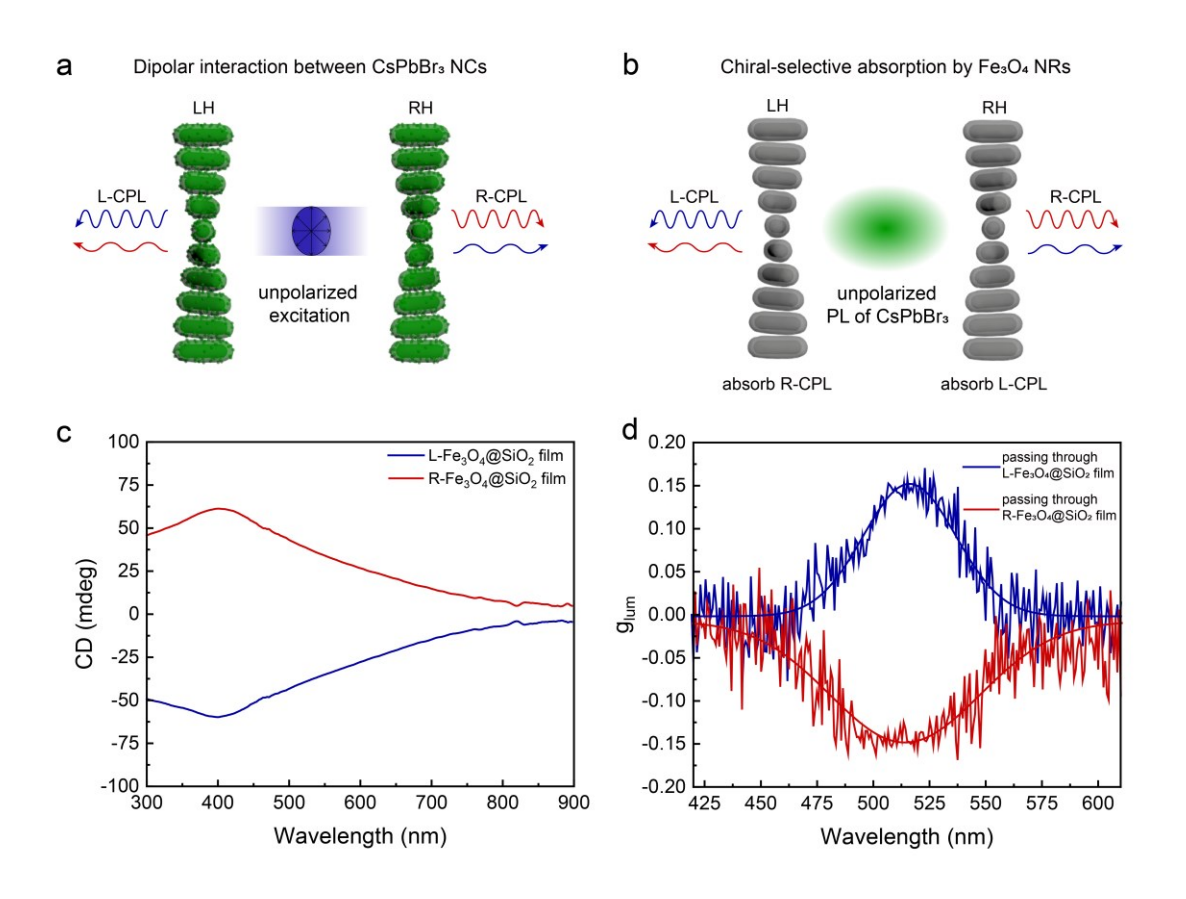


Figure 7. (a) Scheme illustrating the origin of CPL from the dipolar interaction between CsPbBr₃ nanocrystals attached to the chiral nanorod assemblies. (b) Scheme illustrating the origin of CPL from the chiral-selective absorption of CsPbBr₃ emission by Fe₃O₄ in the chiral nanorod assemblies. (c) CD spectra of L- and R-Fe₃O₄@SiO₂ films. (d) g_{lum} of CsPbBr₃ unpolarized light passing through L- and R-Fe₃O₄@SiO₂ films.

In another possible mechanism, CPL may originate from the chiral-selective absorption of the emission by Fe₃O₄ in the chiral assemblies of nanorods (Figure 7b). Even if the original emission is unpolarized, the chiral assemblies of Fe₃O₄ will serve as a chiral-selective filter to release the remanent polarized luminescence. To investigate this possibility, we fabricated L- and R-Fe₃O₄@SiO₂ films by fixing the nanorods in left-handed and right-handed positions, respectively. As shown in Figure 7c, L-Fe₃O₄@SiO₂ film absorbed right-handed light and exhibited a negative CD signal, while R-Fe₃O₄@SiO₂ film absorbed left-handed light and exhibited a positive CD signal. When unpolarized emission from CsPbBr₃ passed through the L-Fe₃O₄@SiO₂ film, a positive g_{lum} could be observed. Conversely, when unpolarized emission from CsPbBr₃ passed through the R-Fe₃O₄@SiO₂ film, a negative g_{lum} could be obtained (Figure 7d). As a result, the CPL of CsPbBr₃ exhibits a polarity preference opposite to the CD signals. This study confirms that the chiral assemblies of Fe₃O₄@SiO₂ nanorods can function as selective absorbers to induce CPL from CsPbBr₃ nanocrystals.

Determining which mechanism plays a dominant role is challenging, but we believe the two mechanisms likely work together to create a strong CPL. On the one hand, the dipolar interaction of the CsPbBr₃ nanocrystals generates preferential emission with a handedness consistent with the chirality of the superstructures. On the other hand, some non-interacting CsPbBr₃ nanocrystals

may also exist in the system, producing unpolarized luminescence. The unpolarized luminescence is then filtered by the chiral superstructures through the selective absorption of iron oxide, leading to CPL with a handedness that matches the chirality of the superstructures. It is thus conceivable that the strong CPL arises as a combined outcome of both mechanisms.

3 Conclusion

We have demonstrated the magnetothermal synthesis of Fe₃O₄@SiO₂/CsPbBr₃ hybrid nanorods and their magnetic assembly into superstructures capable of emitting linear or circularly polarized photoluminescence. The unique magnetothermal process enables the efficient deposition of CsPbBr₃ NCs of controllable loading density to the surface of Fe₃O₄@SiO₂ nanorods. By exposing their colloidal solution to a parallel magnetic field formed using two permanent magnets with opposing poles, the hybrid nanorods assembled into superstructures exhibiting linearly polarized PL emissions with a polarization ratio of 0.10 (± 0.002). Under the chiral field of a cubic permanent magnet, the hybrid nanorods were assembled into chiral superstructures, exhibiting positiondependent CPL with a maximum glum value of 0.44 (±0.004). Further, we revealed two mechanisms that may contribute to the CPL of the chiral assemblies. The first one involves the dipolar interaction between perovskite NCs assembled into chiral structures. In the second mechanism, chiral Fe₃O₄@SiO₂ assemblies selectively absorb one polarized component from the original unpolarized emission of perovskite NCs, promoting polarized emission with complementary chirality. This work showcases the efficacy of magnetic fields in synthesizing and assembling nanostructured materials endowed with distinctive chiroptical properties. These advanced nanomaterials hold great promise for applications spanning diverse fields, including sensors and advanced displays.

Supporting Information

Supporting Information is available from the Wiley Online Library or from the author.

Acknowledgements

The authors are grateful for the financial support from the U.S. National Science Foundation (CHE- 2203972).

Data Availability

The data that support the findings of this study are available from the corresponding author upon reasonable request.

Received: ((will be filled in by the editorial staff))

Revised: ((will be filled in by the editorial staff))

Published online: ((will be filled in by the editorial staff))

References

[1] G. Long, R. Sabatini, M. I. Saidaminov, G. Lakhwani, A. Rasmita, X. Liu, E. H. Sargent, W. Gao,

- Nat. Rev. Mater. 2020, 5, 423.
- [2] Y. Yang, R. C. da Costa, M. J. Fuchter, A. J. Campbell, Nat. Photonics 2013, 7, 634.
- [3] J. R. Brandt, F. Salerno, M. J. Fuchter, Nat. Rev. Chem. 2017, 1, 0045.
- [4] C. Ye, J. Jiang, S. Zou, W. Mi, Y. Xiao, J. Am. Chem. Soc. 2022, 144, 9707.
- [5] S. Feuillastre, M. Pauton, L. Gao, A. Desmarchelier, A. J. Riives, D. Prim, D. Tondelier, B. Geffroy, G. Muller, G. Clavier, G. Pieters, J. Am. Chem. Soc. 2016, 138, 3990.
- [6] M. C. Heffern, L. M. Matosziuk, T. J. Meade, Chem. Rev. 2014, 114, 4496.
- [7] H. K. Bisoyi, Q. Li, Acc. Chem. Res. 2014, 47, 3184.
- [8] X.-K. Liu, W. Xu, S. Bai, Y. Jin, J. Wang, R. H. Friend, F. Gao, *Nat. Mater.* **2021**, 20, 10.
- [9] Y. Su, Q. Jing, Y. Xu, X. Xing, Z. Lu, ACS Omega 2019, 4, 22209.
- [10] Q. Jing, Y. Su, X. Xing, Z. Lu, J. Mater. Chem. C 2019, 7, 1854.
- [11] S. W. Eaton, M. Lai, N. A. Gibson, A. B. Wong, L. Dou, J. Ma, L.-W. Wang, S. R. Leone, P. Yang, Proc. Natl. Acad. Sci. U. S. A. 2016, 113, 1993.
- [12] P. Ramasamy, D.-H. Lim, B. Kim, S.-H. Lee, M.-S. Lee, J.-S. Lee, *Chem. Commun.* **2016**, 52, 2067.
- [13] X. Li, D. Yu, J. Chen, Y. Wang, F. Cao, Y. Wei, Y. Wu, L. Wang, Y. Zhu, Z. Sun, J. Ji, Y. Shen,H. Sun, H. Zeng, ACS Nano 2017, 11, 2015.
- [14] Z. Wang, L. Zeng, T. Zhu, H. Chen, B. Chen, D. J. Kubicki, A. Balvanz, C. Li, A. Maxwell, E. Ugur, R. dos Reis, M. Cheng, G. Yang, B. Subedi, D. Luo, J. Hu, J. Wang, S. Teale, S. Mahesh, S. Wang, S. Hu, E. D. Jung, M. Wei, S. M. Park, L. Grater, E. Aydin, Z. Song, N. J. Podraza, Z.-H. Lu, J. Huang, V. P. Dravid, S. De Wolf, Y. Yan, M. Grätzel, M. G. Kanatzidis, E. H. Sargent, *Nature* 2023, 618, 74.
- [15] R. Lin, Y. Wang, Q. Lu, B. Tang, J. Li, H. Gao, Y. Gao, H. Li, C. Ding, J. Wen, P. Wu, C. Liu, S. Zhao, K. Xiao, Z. Liu, C. Ma, Y. Deng, L. Li, F. Fan, H. Tan, *Nature* 2023, 620, 994.
- [16] Y.-H. Kim, Y. Zhai, E. A. Gaulding, S. N. Habisreutinger, T. Moot, B. A. Rosales, H. Lu, A. Hazarika, R. Brunecky, L. M. Wheeler, J. J. Berry, M. C. Beard, J. M. Luther, *ACS Nano* **2020**, 14,

8816.

- [17] M. Naito, K. Iwahori, A. Miura, M. Yamane, I. Yamashita, Angew. Chem., Int. Ed. 2010, 49, 7006.
- [18] Y. Shi, P. Duan, S. Huo, Y. Li, M. Liu, Adv. Mater. **2018**, 30, 1705011.
- [19] P. Liu, W. Chen, Y. Okazaki, Y. Battie, L. Brocard, M. Decossas, E. Pouget, P. Müller-Buschbaum, B. Kauffmann, S. Pathan, T. Sagawa, R. Oda, *Nano Lett.* **2020**, 20, 8453.
- [20] X. Zhang, Y. Xu, C. Valenzuela, X. Zhang, L. Wang, W. Feng, Q. Li, Light: Sci. Appl. 2022, 11, 223.
- [21] Z. Li, Q. Fan, Z. Ye, C. Wu, Z. Wang, Y. Yin, Science 2023, 380, 1384.
- [22] Z. Ye, Z. Li, J. Feng, C. Wu, Q. Fan, C. Chen, J. Chen, Y. Yin, ACS Nano 2023, 17, 18517.
- [23] C. Wu, Q. Fan, W. Wu, T. Liang, Y. Liu, H. Yu, Y. Yin, Nano Lett. 2023, 23, 1981.
- [24] Z. Wang, D. Schnable, Q. Fan, Z. Li, G. Ung, Y. Yin, ACS Nano 2024, 18, 5122.
- [25] Q. Fan, Z. Li, C. Wu, Y. Yin, Precis. Chem. 2023, 1, 272.
- [26] Z. Li, J. Jin, F. Yang, N. Song, Y. Yin, Nat. Commun. 2020, 11, 2883.
- [27] L. Protesescu, S. Yakunin, M. I. Bodnarchuk, F. Krieg, R. Caputo, C. H. Hendon, R. X. Yang, A. Walsh, M. V. Kovalenko, *Nano Lett.* **2015**, 15, 3692.
- [28] A. E. Deatsch, B. A. Evans, J. Magn. Magn. Mater. 2014, 354, 163.
- [29] Z. Li, M. Kawashita, N. Araki, M. Mitsumori, M. Hiraoka, M. Doi, *Mater. Sci. Eng. C* 2010, 30, 990.
- [30] T. Dong, J. Zhao, G. Li, F.-C. Li, Q. Li, S. Chen, ACS Appl. Mater. Interfaces 2021, 13, 39748.

Table of Contents

Chiral superstructures with polarized emission are created through a two-step process, involving first the magnetothermal synthesis of magnetite/perovskite hybrid nanorods and then their assembly in external magnetic fields. The resulting superstructures exhibit linear or circularly polarized emission, depending on the chirality of the magnetic fields.

Yucong Su, Yuchen Zhang, Zuyang Ye, Jolene Cao, Qingsong Fan, Xinchao Wang, Chen Chen, Yun Liu, Zhongxiang Wang, Zhenda Lu, and Yadong Yin*

Magnetic Assembly of Magnetite/Perovskite Hybrid Nanorods for Circularly Polarized Luminescence

